Control Strategy for an Integrated Photovoltaic-Battery System

Andoni Urtasun, Pablo Sanchis and Luis Marroyo
Department of Electrical and Electronic Engineering
Institute of Smart Cities
Public University of Navarre (UPNA)
Pamplona, Spain

Acknowledgments

This work was supported by the Spanish State Research Agency (AEI) and FEDER-UE under grants DPI2013-42853-R and DPI2016-80641-R. The authors gratefully acknowledge the financial and ongoing support of INGETEAM POWER TECHNOLOGY.

Keywords

«Battery charger», «Energy system management», «Microgrid», «Photovoltaic», «Renewable energy systems».

Abstract

In photovoltaic-battery systems, more attention is usually paid to the MPPT control while the battery management is put aside. This paper proposes two control strategies for an integrated PV-battery system, both of them making it possible to perform MPPT or regulate the battery voltage to its maximum value in order to prevent it from overcharging. Simulation results prove the feasibility of both controls.

1. Introduction

Photovoltaic (PV) capacity is growing very quickly thanks to its increasingly competitive prices. Due to the intermittent nature of the photovoltaic sources, battery energy storage can be included in the system in order to contribute to improve grid integration and allow for stand-alone operation in case of grid failure.

For low-power PV-battery systems (less than 10 kW), a number of configurations are found in the industry and literature, as shown in Fig. 1. In the first configuration (Fig. 1(a)), the PV generator and the battery are connected to the grid by means of two inverters [1], [2]. If battery and PV voltages are not high enough, two-stage inverters including a dc/dc boost converter as the first stage are employed. This configuration permits a high versatility to place the PV generator and the battery in different locations, at the expense of lower conversion efficiency and higher cost.

If the PV generator and the battery are close to each other, such as in household applications, then the configurations shown in Fig. 1(b)-(d) are more convenient. In the structure shown in Fig. 1(b), the PV generator and the battery are connected to the dc bus through two dc/dc boost converters and then a single inverter is required for grid connection [3]. The conversion efficiency and cost can be further improved by using a dual-input dc/dc converter, as shown in Fig. 1(c) [4]. Alternatively, the battery [5] or the PV generator [6], [7], could be directly placed at the dc bus. Since a high enough voltage is required at the input of the step-down inverter, the configuration shown in Fig. 1(d), with the PV generator in the dc bus, is usually preferred. This configuration is the most cost-effective, and the PV power is processed by only one converter, resulting in a higher conversion efficiency.

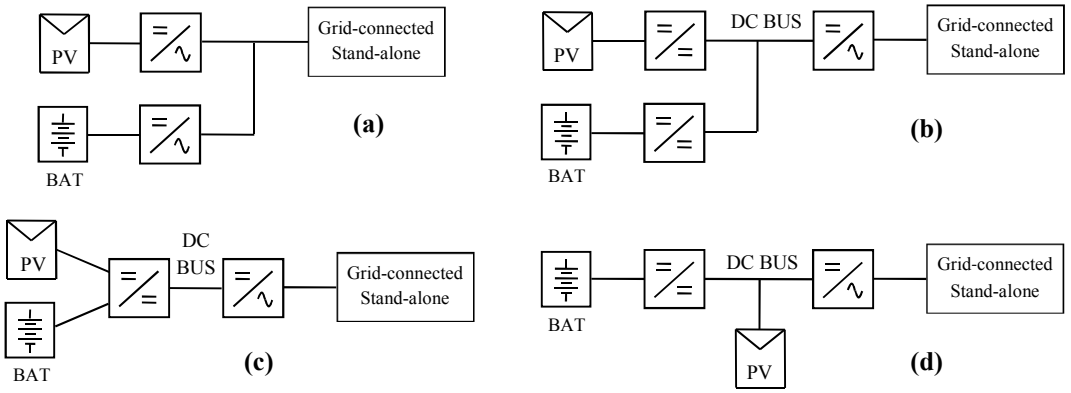

Fig. 1. Conversion configurations for PV-battery systems: (a) PV and battery connected in ac, (b) PV and battery connected in dc, (c) PV and battery connected to a dual-input dc/dc converter, (d) PV connected to the dc bus.

Some authors have analyzed the control of the latter configuration, showing how to control the dc bus voltage in order to perform Maximum Power Point Tracking (MPPT) [7]. However, the battery management for this system has not been tackled. In particular, in order to extend the battery lifetime, it is of the utmost importance to regulate the battery voltage to its maximum value in order to prevent it from overcharging. Thus, under stand-alone operation, where the extra PV power cannot be injected into the grid, the MPPT algorithm must be cancelled and the PV power reduced, allowing for battery protection.

This paper presents two different control strategies for the PV-battery system under stand-alone operation. Both strategies make it possible to maximize or reduce the PV power as required, performing MPPT as far as possible or controlling the battery voltage to its maximum value when necessary. The control during MPPT operation, which is common for both strategies, is first analyzed in the paper. The features of each strategy are then presented, and simulation results are provided in the last section.

2. Control strategies

Control during MPPT operation

The analyzed system is shown in Fig. 2 under stand-alone operation. It consists of a battery, a boost converter, a PV generator, a bus capacitor, and a single-phase inverter. The parameters of the system under study are shown in Table I, where the values for the PV generator are given at Standard Test Conditions (STC). In this scheme, the power balance is as follows:

$$P_{ac} = P_{bat} + P_{pv}\,, \tag{1}$$

where P_{ac} is the load power, P_{pv} the PV power and P_{bat} the power delivered by the battery.

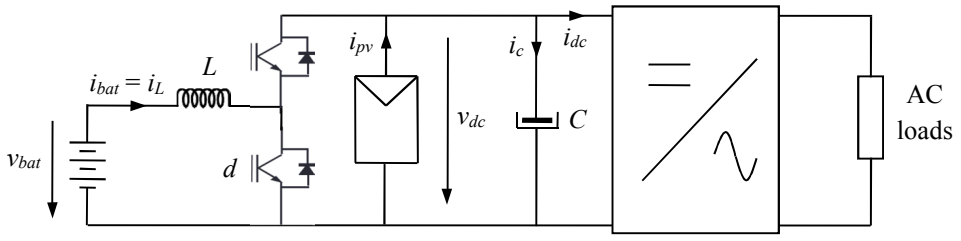

Fig. 2. PV-battery system with the PV generator connected to the dc bus, under stand-alone operation.

Table I. Parameters of the PV-battery system.

Battery nominal voltage	240 V
Battery maximum voltage	280 V
Boost converter inductance	750 µH
Boost converter rated current	25 A
Bus capacitance	2.5 mF
PV generator peak power at STC	9 kWp
PV generator MPP voltage at STC	380 V
PV generator MPP current at STC	23.7 A
Grid rated voltage	230 V
Inverter rated power	6 kVA

There are two cascaded regulations, one for the inverter and one for the boost converter. The inverter controls the grid voltage by means of an inner current loop, thus supplying the power required by the load [8].

This paper deals with the regulation of the boost converter. Its control scheme during MPPT operation is shown in Fig. 3, consisting of an MPPT algorithm, an outer dc voltage loop, and an inner inductor current loop. In the figure, subscript f represents variables which have been measured and filtered, superscript * represents reference variables, $G_{i,cl}$ represents the inductor current closed-loop and H_{Vdc} the dc voltage moving-average filter used to remove the component at twice the grid frequency. The MPPT used here is a typical perturbation and observation algorithm [9], which uses measured variables $v_{dc,f}$, $P_{ac,f}$ and $P_{bat,f}$ in order to obtain the voltage reference v^*_{dc}. In both voltage and current loops, a PI controller and feedforward compensations with measured variables are used.

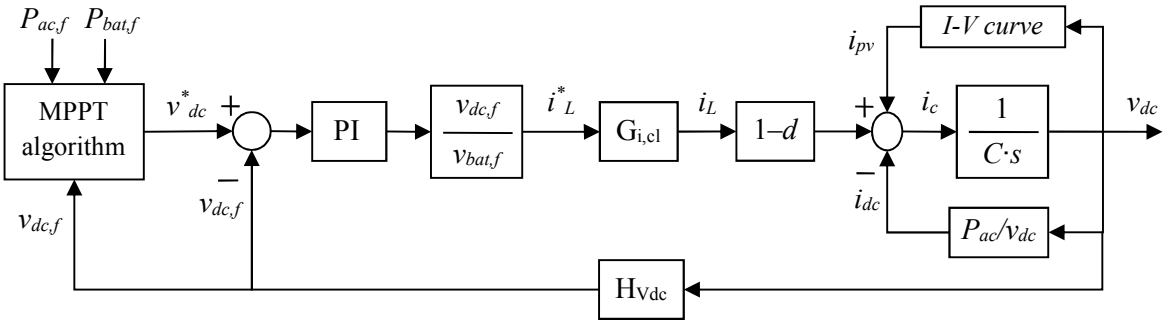

Fig. 3. Boost converter control loop during MPPT operation.

The current control with feedforward compensations for a boost converter is widely known and can be consulted in [10]. Concerning the dc voltage regulation, although the output voltage control for a boost converter has also been analyzed in the literature, the effect of the PV generator non-linear behavior on the control is not usually taken into account. In order to design the dc voltage control loop, the inductor current to dc voltage transfer function should be determined. From Fig. 2, inductor current and dc voltage variations can be obtained as

$$L \cdot \frac{di_L}{dt} = v_{bat} - (1-d) \cdot v_{dc}, \tag{2}$$

$$C \cdot \frac{dv_{dc}}{dt} = (1-d) \cdot i_L + i_{pv} - i_{dc}. \tag{3}$$

Applying the Laplace transformation and small-signal analysis to (2) and (3) yields to:

$$Ls \cdot \hat{i}_L = \hat{v}_{bat} - (1-D) \cdot \hat{v}_{dc} + V_{dc} \cdot \hat{d}\,, \tag{4}$$

$$Cs \cdot \hat{v}_{dc} = (1-D) \cdot \hat{i}_L - I_L \cdot \hat{d} + \hat{i}_{pv} - \hat{i}_{dc}\,, \tag{5}$$

where small-signal variables are marked with a circumflex and the steady-state values are capitalized.

Since the inverter control includes v_{dc} feedforward compensation, v_{dc} variation has no effect on the ac side and the inverter can be considered as constant power load. As a result, the following applies:

$$v_{dc} \cdot i_{dc} = P_{ac} \quad \Rightarrow \quad \hat{i}_{dc} = -\frac{P_{ac}}{V_{dc}^2} \cdot \hat{v}_{dc}\,. \tag{6}$$

Similarly, from the I-V curve, the small-signal PV current can be obtained as [11]

$$\hat{i}_{pv} = -\frac{1}{R_{pv}} \cdot \hat{v}_{dc}\,, \tag{7}$$

where R_{pv} is the PV dynamic resistance, which is related to the I-V curve slope. The dynamic resistance is very variable depending on the operating point, with low values at open-circuit voltage and high values near short-circuit.

Introducing (6) and (7) into (5), and operating in (4) and (5), it is possible to obtain the inductor current to dc voltage transfer function as

$$G_{IL-Vdc} = \frac{\hat{v}_{dc}}{\hat{i}_L} = \frac{V_{bat}}{V_{dc}} \cdot \frac{-s/\omega_z + 1}{C \cdot (s - \omega_p)}\,, \tag{8}$$

$$\omega_z = \frac{V_{bat}}{L \cdot I_L}\,, \quad \omega_p = \frac{1}{C} \cdot \left(\frac{P_{pv}}{V_{dc}^2} - \frac{1}{R_{pv}} \right). \tag{9}$$

As can be observed, this transfer function includes the following features:

- A variable gain V_{bat}/V_{dc}, which will be compensated by the feedforward term $v_{dc,f}/v_{bat,f}$ (see Fig. 3).
- A Right-Half-Plane (RHP) zero at ω_z, which limits the voltage control bandwidth to about $\omega_z/5$ [12]. However, this is not a limitation in this application since the dc voltage control in single-phase systems needs to be slow due to the component at twice the grid frequency.
- A variable pole at ω_p, which is situated in the RHP when positive and in the Left-Half-Plane (LHP) when negative. As can be seen in (9), this pole is due to the PV generator but in two different ways. The term $1/R_{pv}$ is related to the resistive behavior of the PV generator, which decreases its current when its voltage increases, helping to damp the system and moving the pole towards the LHP. On the other hand, the term P_{pv}/V^2_{dc} represents that the inverter power is always higher than the battery power ($P_{ac} - P_{bat} = P_{pv}$). As a result, the damping effect of the boost converter, as a constant power source, is always lower than the undamping effect of the inverter, as a constant power load, contributing to move the pole towards the RHP.

The non-compensated open-loop transfer function can thus be obtained as

$$G_{IL-Vdc} \cdot G_{i,cl} \cdot H_{Vdc} = \frac{\hat{v}_{dc,f}}{\hat{i}_L^*} = \frac{V_{bat}}{V_{dc}} \cdot \frac{-s/\omega_z + 1}{C \cdot (s - \omega_p)} \cdot \frac{1}{s/\omega_v + 1}\,, \tag{10}$$

where, for the frequencies of concern (around and below the crossover frequency, $f_c \approx 15$ Hz), $G_{i,cl}$ can be considered as 1 and H_{Vdc} as a first-order low-pass filter with ω_v as the angular cutoff frequency.

Figure 4 shows the bode plot of the non-compensated open-loop transfer function for three f_p values ($f_p = \omega_p/2\pi$) representing three operating points. The case with $f_p = 0$ represents the situation in which there is no PV generator or it is not illuminated. The case with $f_p = 40$ Hz (in the LHP) occurs at open-circuit voltage, where $P_{pv} = 0$ and R_{pv} is minimum [see (9)]. As can be observed in the figure, the phase is higher but the gain is lower when compared to the curve for $f_p = 0$. Finally, $f_p = 6$ Hz (in the RHP) occurs with a dc voltage slightly lower to the MPP voltage, where P_{pv} and R_{pv} are high. In this case, the phase is very low due to the RHP pole. As a result, in order to guarantee stability, this operating point should be considered in order to design the voltage controller. When using a PI controller, the crossover frequency is very restricted because it should be over the RHP pole (at 6 Hz) but below the filter pole (32 Hz). Thus, the PI controller is designed here to have a crossover frequency $f_c = 15$ Hz, and a phase margin PM = 37º for the operating point with $f_p = 6$ Hz (RHP).

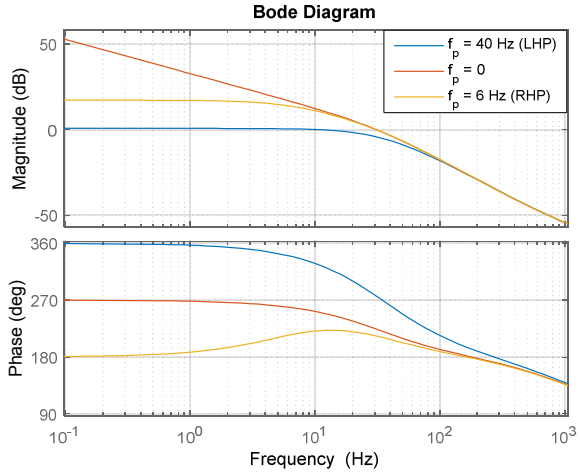

Fig. 4. Non-compensated open-loop transfer function, $G_{IL\text{-}Vdc} \cdot G_{i,cl} \cdot H_{Vdc}$, for three operating points.

However, the voltage loop dynamic properties are dependent on the operating point due to the influence of the PV generator. This can be observed in Fig. 5, where the crossover frequency and phase margin are plotted as a function of the operating point. In particular, it should be noted that regulation becomes slower near open-circuit voltage and that stability is ensured in all situations.

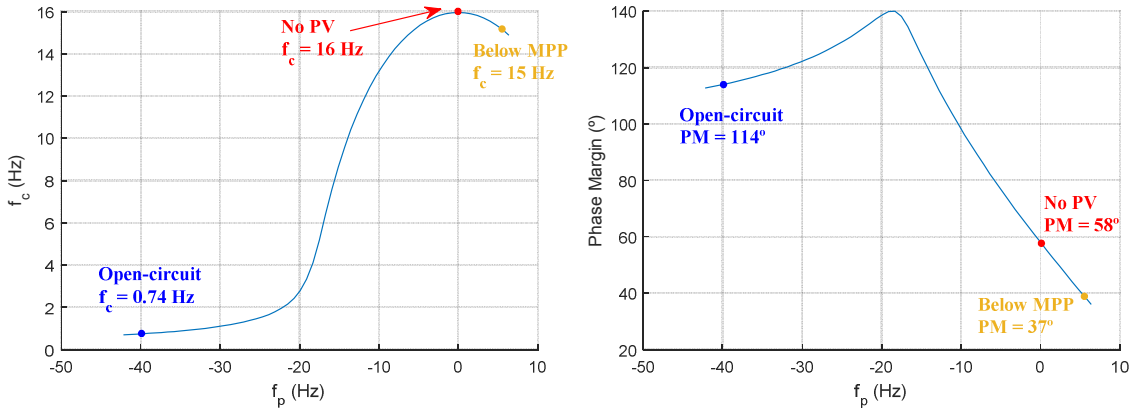

Fig. 5. Crossover frequency and phase margin of dc voltage regulation for different operating points.

The control presented up to now, as shown in Fig. 3, is valid for MPPT operation, as far as the battery can handle the net power, $P_{bat} = P_{ac} - P_{pv}$. However, when the battery is fully charged, its voltage can

exceed the maximum value and then the PV power must be reduced in order avoid overcharging. For this purpose, two methods which include the battery voltage regulation are proposed below.

Control strategy 1: increase of the dc voltage

In the first strategy, shown in Fig. 6, two dc voltage references are obtained, namely $v_{dc,mppt}$, dedicated to maximize the PV power, and $v_{dc,lim}$, to reduce the PV power and control the battery voltage. Then, the control selects the dc voltage reference as the highest between these two values. As a result, when the battery voltage is below its maximum value, $v_{dc,lim}$ is saturated to the minimum dc voltage and the MPPT algorithm is thus active. On the other hand, when the battery voltage exceeds its reference value, the reference $v_{dc,lim}$ increases over $v_{dc,mppt}$ and the control increases v_{dc} in order to reduce the PV power, making it possible to control the battery voltage. Due to the non-linear P-V curve of the PV generator and to the dc voltage closed-loop properties, the plant for the battery voltage control is variable and the response strongly depends on the operating point.

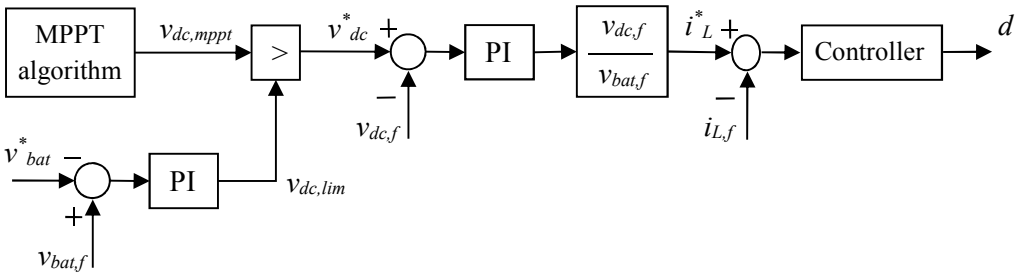

Fig. 6. Boost converter control loop for both MPPT and limitation modes: Increase of the dc voltage.

In order to obtain the dc voltage to battery voltage transfer function, a small-signal power balance is first applied:

$$\hat{p}_{bat} = \hat{p}_{ac} - \hat{p}_{pv} . \tag{11}$$

Considering the small-signal model of the battery as a pure resistance R_{bat} [13], and (7), the PV and battery powers can be obtained as

$$\hat{p}_{pv} = -\left(\frac{V_{dc}}{R_{pv}} - I_{pv} \right) \cdot \hat{v}_{dc} = -K_{pv} \cdot \hat{v}_{dc} , \tag{12}$$

$$\hat{p}_{bat} = -\left(\frac{V_{bat}}{R_{bat}} - I_{L} \right) \cdot \hat{v}_{dc} = -K_{bat} \cdot \hat{v}_{bat} , \tag{13}$$

where K_{pv} and K_{bat} are related to the slope of their respective P-V curves. Parameter K_{pv} is very variable in operation, changing from 0 at MPP voltage to a large value at open-circuit voltage. In the case of parameter K_{bat}, its variation range for a predetermined battery is less important and can be disregarded.

From (11)–(13) and taking into account that P_{ac} is only dependent on the ac side, the dc voltage to battery voltage transfer function is obtained as

$$G_{Vdc-Vbat} = \frac{\hat{v}_{bat}}{\hat{v}_{dc}} = -\frac{K_{pv}}{K_{bat}} \cdot \tag{14}$$

Similarly to the dc voltage regulation and, as made clear by this expression, the battery voltage regulation is also dependent on the PV generator non-linear behavior. The non-compensated open-loop transfer function can now be obtained as

$$G_{Vdc-Vbat} \cdot G_{Vdc,cl} \cdot H_{Vbat} = \frac{\hat{v}_{bat,f}}{\hat{v}_{dc}^{*}} = -\frac{K_{pv}}{K_{bat}} \cdot \frac{C_{Vdc} \cdot G_{IL-Vdc} \cdot G_{i,cl}}{1 + C_{Vdc} \cdot G_{IL-Vdc} \cdot G_{i,cl} \cdot H_{Vdc}} \cdot H_{Vbat}, \quad (15)$$

where $G_{Vdc,cl}$ represents the dc voltage closed-loop, H_{Vbat} the battery voltage low-pass filter and C_{Vdc} the dc voltage PI controller.

This transfer function bode plot is depicted in Fig. 7 (left side) for three operating points: at open-circuit voltage, at a voltage between open-circuit and MPP, and slightly over MPP voltage. As can be observed, the gain strongly depends on the operating point. Obviously, the open-loop gain is much higher near open-circuit since K_{pv} is larger, meaning that a dc voltage variation causes a high PV power reduction. Furthermore, the influence of the dc voltage closed-loop on the battery voltage regulation can also be analyzed from the figure (left side). It shows that the phase remains over 315º up to 20 Hz, even when operating at open-circuit voltage, at which the inner dc voltage loop has a crossover frequency of 0.74 Hz (see Fig. 5). The bode plot of the compensated open-loop is also shown in Fig. 7 (right side), including a PI controller designed to have a maximum crossover frequency of 10 Hz. As can be observed, this dynamics is obtained at open-circuit voltage however the battery voltage response becomes slower as the PV voltage moves towards MPP voltage.

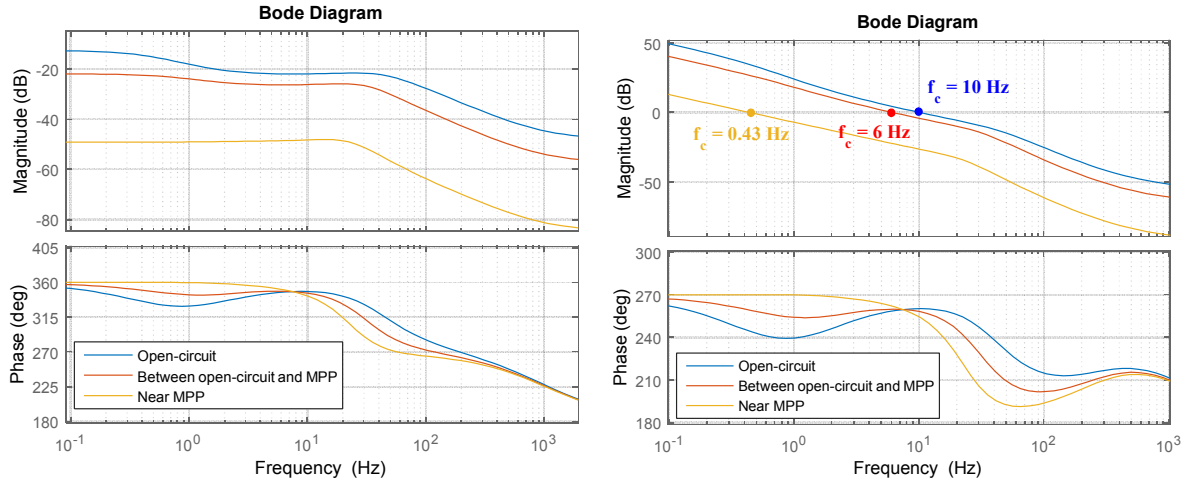

Fig. 7. Non-compensated (left side) and compensated (right side) open loop transfer function for the battery voltage regulation, for three operating points.

Control strategy 2: reduction of the battery charging current

In the case of the second strategy, as shown in Fig. 8, two inductor current references are determined, namely $i_{L,mppt}$, dedicated to control the dc voltage and maximize the PV power, and $i_{L,lim}$, to reduce the PV power and control the battery voltage. Then, the inductor current reference is chosen as the highest one. According to this strategy, when the battery voltage is below its reference, $i_{L,lim}$ remains saturated to the minimum value, $-I_{max}$, meaning that the maximum charging current is permitted. As a result, the MPPT algorithm is active and the battery delivers the current $i_L = i_{L,mppt}$, which can be positive (for discharging) or negative (for charging), depending on generation and consumption. Alternatively, when the battery voltage exceeds its reference value, the reference $i_{L,lim}$ increases over $i_{L,mppt}$. Since $i_{L,lim}$ is always negative, a reduction in the charging current is carried out, which in turn makes it possible to control the battery voltage by means of a PV power reduction.

With this strategy, during limitation mode, the inductor current directly controls the battery voltage. As a result, the system plant is only related to the battery and not to the PV generator. In particular, the

inductor current to battery voltage transfer function is the battery impedance Z_{bat}, which can be approximated as a resistance for the frequencies of concern [13]:

$$G_{IL-Vbat} = \frac{\hat{v}_{bat}}{\hat{i}_L} = -Z_{bat} \approx -R_{bat} \,. \tag{16}$$

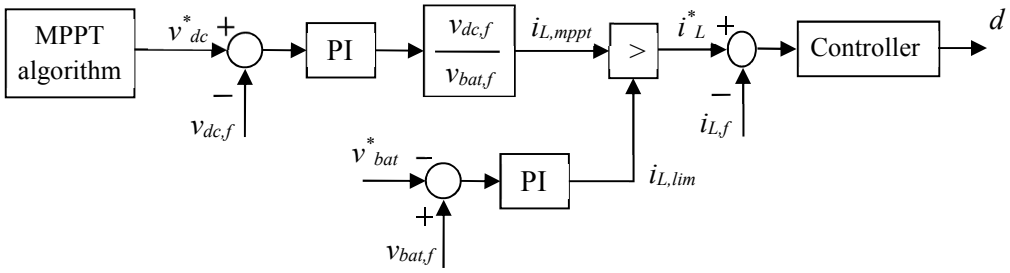

Fig. 8. Boost converter control loop for both MPPT and limitation modes: Reduction of the battery charging current.

On account of the system plant, the PI controller is designed to have a crossover frequency of 10 Hz. Then, in operation, the battery voltage response will remain similar for all operating point since it is now independent of the PV array non-linear features.

Finally, it is also worth noting that, in limitation mode, the dc voltage is not controlled. In this situation, the extra PV power will be absorbed by the dc capacitor, causing a dc voltage increase and a PV power reduction until reaching the steady-state, with the dc voltage always being below the open-circuit value.

3. Results

Both control strategies are tested by using the simulation software PSIM. The model includes the battery, a boost converter, the PV generator, and a single-phase inverter connected to the loads. The parameters of the system under study were shown in Table I. During the simulations, the irradiance is 900 W/m^2 and the cell temperature 40ºC, which gives a maximum PV power of P_{MPP} = 7.8 kW, and a number of loads are connected and disconnected.

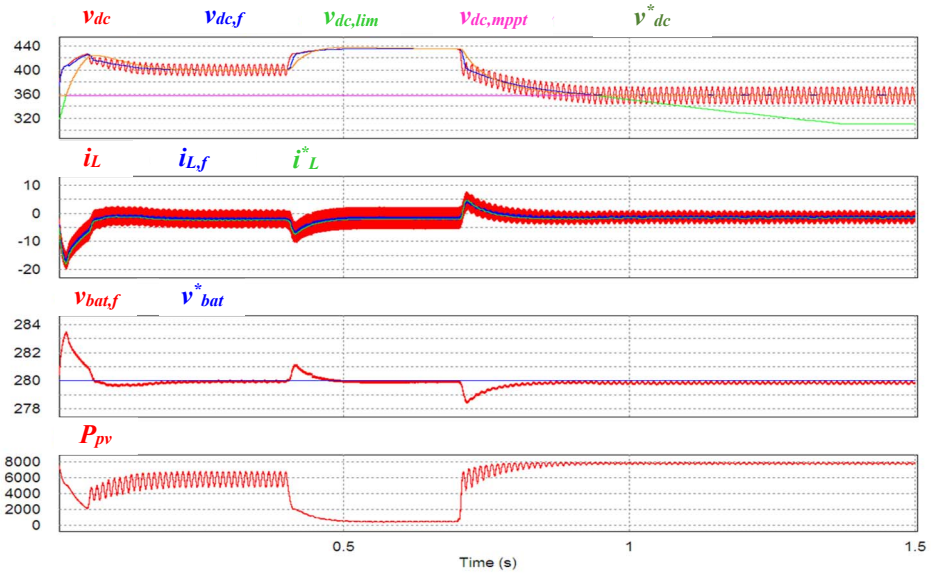

Fig. 9. Simulation results for the first control strategy.

The simulation results for the first strategy (see Fig. 6) are shown in Fig. 9. At the beginning, a 5.2 kW load is connected. This power is lower than the photovoltaic power and, as a result, the battery absorbs the difference. Since the battery is fully charged, its voltage exceeds the reference value, leading to an increase in the reference $v_{dc,lim}$. When $v_{dc,lim}$ gets over $v_{dc,mppt}$, $v_{dc,lim}$ is selected as the actual reference and is controlled by means of the inner current loop. The outcome is that the battery voltage is regulated thanks to a PV power reduction. Afterwards, all loads are disconnected, resulting in an increase of the battery charging current and voltage. The battery voltage controller thus increases again the dc voltage in order to further reduce the PV power, making it possible to control the battery voltage. Finally, a 7.9 kW load is connected, leading to a battery discharge. In this situation, the battery voltage decreases below the reference value and the controller then reduces the dc voltage reference until the system switches to MPPT mode.

The simulation results for the second strategy (see Fig. 8) are shown in Fig. 10. At the beginning, a 5.2 kW load is connected and the system is under MPPT mode. Then, at about second 0.4, the load is disconnected. Since the battery is fully charged, its voltage rises over the reference value and, according to the control, the current reference $i_{L,lim}$ is increased. When $i_{L,lim}$ gets over $i_{L,mppt}$, $i_{L,lim}$ is selected as the actual reference, making it possible to regulate the battery voltage. In this situation, the dc voltage is not controlled but evolves towards PV voltage required to supply the necessary PV power. Finally, the 5.2 kW load is again connected. Then, as a result of the control, the battery $i_{L,mppt}$ gets over $i_{L,lim}$ and the operating mode switches to MPPT.

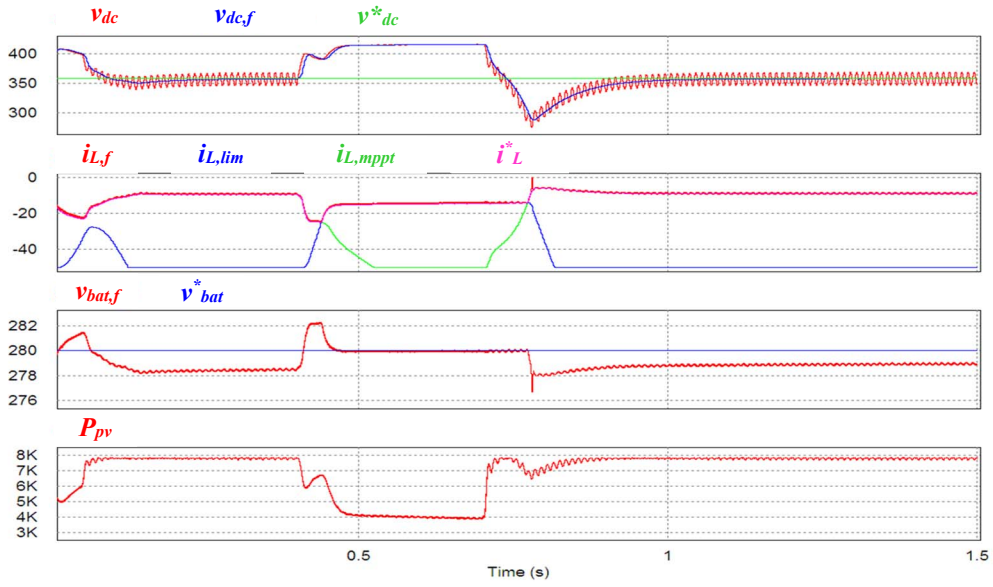

Fig. 10. Simulation results for the second control strategy.

4. Conclusions

This paper presents two control strategies for an integrated photovoltaic-battery system, putting emphasis on the battery voltage regulation when the battery is fully charged and the extra PV power cannot be consumed. In this situation, the only solution is to reduce the PV power, which can be realized in two manners, either by increasing the PV voltage reference or by directly decreasing the charging current of the battery.

The first strategy is more complicated since it requires three cascaded feedback loops operating at the same time. Furthermore, the battery voltage regulation has variable dynamics depending on the PV generator operating point. On the other hand, the second strategy is simpler to implement as only two

cascaded feedback loops are required. Besides, the battery voltage regulation is fast enough for every operating point since the influence of the PV generator non-linearity is avoided.

The feasibility of both control strategies has been proved by simulation results.

References

[1] A. Urtasun, E. L. Barrios, P. Sanchis, and L. Marroyo, "Frequency-based energy-management strategy for stand-alone systems with distributed battery storage," *IEEE Trans. Power Electron.*, vol. 30, no. 9, pp. 4794–4808, Sep. 2015.

[2] A. Urtasun, P. Sanchis, and L. Marroyo, "State-of-charge-based droop control for stand-alone AC supply systems with distributed energy storage," *Energy Conversion and Management*, vol. 106, pp. 709–720, Dec. 2015.

[3] Y. Mei, and X. Li, "A new control method of balancing inductor current for interleaved parallel bi-directional DC-DC converter," in *8th Int. Power Electron. and Motion Control Conf.*, pp. 2988–2992, May 2016.

[4] F. Guo, L. Fu, X. Zhang, C. Yao, H. Li, and J. Wang, "A family of quasi-switched-capacitor circuit-based dual-input DC/DC converters for photovoltaic systems integrated with battery energy storage," *IEEE Trans. Power Electron.*, vol. 31, no. 12, pp. 8237–8246, Dec. 2016.

[5] M. Rezkallah, A. Hamadi, A. Chandra, and B. Singh, "Real-time HIL implementation of sliding mode control for standalone system based on PV array without using dumpload," *IEEE Trans. Sust. Energy*, vol. 6, no. 4, pp. 1389–1398, Oct. 2015.

[6] R. Gules, J. P. Pacheco, H. L. Hey, and J. Imhoff, "A maximum power point tracking system with parallel connection for PV stand-alone applications," *IEEE Trans. Ind. Electron.*, vol. 55, no. 7, pp. 2674–2683, Jul. 2008.

[7] D. Velasco de la Fuente, C. L. T. Rodriguez, G. Garcera, E. Figueres, and R. O. Gonzalez, "Photovoltaic power system with battery backup with grid-connection and islanded operation capability," *IEEE Trans. Ind. Electron.*, vol. 60, no. 4, pp. 1571–1581, Apr. 2013.

[8] P. Sanchis, A. Ursua, E. Gubia, J. Lopez, and L. Marroyo, "Control of three-phase stand-alone photovoltaic systems with unbalanced loads," in *2015 Int. Sysmposium on Ind. Electron.*, pp. 633–638, Nov. 2005.

[9] A. K. Abdelsalam, A. M. Massoud, S. Ahmed, and P. N. Enjeti, "High-performance adaptive perturb and observe MPPT technique for photovoltaic-based microgrids," *IEEE Trans. Power Electron.*, vol. 26, no. 4, pp. 1010–1021, 2011.

[10] K. De Gusseme, D. M. Van de Sype, A. P. M. Van den Bossche, and J. A. Melkebeek, "Digitally controlled boost power-factor-correction converters operating in both continuous and discontinuous conduction mode," *IEEE Trans. Ind. Electron.*, vol. 52, no. 1, pp. 88–97, Feb. 2005.

[11] A. Urtasun, P. Sanchis, L. Marroyo, "Adaptive voltage control of the DC/DC boost stage in PV converters with small input capacitors," *IEEE Trans. Power Electron.*, vol. 28, no. 11, pp. 5038–5048, Nov. 2013.

[12] R. B. Ridley, *Power Supply Design, Volume 1: Control*, Ridley Engineering, Inc., ISBN 978-0-9833180-0-2, 2012.

[13] S.-Y. Cho, I.-O. Lee, J.-I. Baek and G.-W. Moon, "Battery impedance analysis considering DC component in sinusoidal ripple-current charging," *IEEE Trans. on Ind. Electron*, vol. 63, no. 3, pp. 1561–1573, Mar. 2016.